JOURNAL OF GUIDANCE, CONTROL, AND DYNAMICS
Vol. 38, No. 8, August 2015

Engineering Notes

Low-Thrust Minimum-Fuel Optimization in the Circular Restricted Three-Body Problem

Chen Zhang*
Beihang University, 100191 Beijing, People's Republic of China
Francesco Topputo† and Franco Bernelli-Zazzera‡
Politecnico di Milano, 20156 Milan, Italy
and
Yu-Shan Zhao§
Beihang University, 100191 Beijing, People's Republic of China

DOI: 10.2514/1.G001080

I. Introduction

THE challenging missions envisioned for the upcoming decades involve innovative spacecraft trajectory concepts. For instance, installing outposts at Earth–moon Lagrange points requires novel transfers. These orbits shall, at minimum, be able to combine the benefits inherent to multibody dynamics with those enabled by advanced propulsion technologies. The three-body dynamics already suffice to produce free transport mechanisms, whereas the high specific impulse typical of low-thrust propulsion allows considerable propellant savings. The challenge is then to design optimal low-thrust three-body transfers.

This subject has recently gained the attention of the scientific community. In [1], design synthesis is achieved by combining invariant manifolds and attainable sets, which are sets containing ballistic and low-thrust orbits, respectively. In [2], transfers to distant periodic orbits have been designed by targeting their invariant manifolds with low-thrust propulsion. Using invariant manifolds as a first-guess solution in high-fidelity low-thrust optimization was examined in [3]. Low-energy low-thrust transfers to the moon were formulated in [4,5]. Low-thrust optimization in a three-body model was also studied in [6–10] without relying on invariant manifolds. These concepts were demonstrated by SMART-1 [11], where the pioneering ideas in [12] were applied.

In this field, the case of low-thrust transfers to Earth–moon Lagrange point orbits is of interest. As the latter are chosen as ideal targets for a number of future applications [13–15], it is crucial to assess their accessibility in terms of cost and time. In doing so, it is worth considering departure from a geostationary transfer orbit (GTO). This orbit is chosen because launch vehicles are optimized for GTO, and the case of piggyback spacecraft may also be accounted for. Nevertheless, finding an optimal low-thrust trajectory from GTO to Lagrange point orbits in the Earth–moon system is particularly challenging because of 1) the long-duration nature of the solutions, 2) the high number of revolutions, 3) the strong nonlinearities in the three-body vector field, and 4) the high number of bang–bang structures in the optimal guidance law. These features have prevented finding end-to-end optimal transfers; and some sorts of approximations, leading to suboptimal solutions, have been favored over optimality. In [16], the transfer orbit is defined by patching together a tangential thrust spiral with a leg targeting a portion of the stable manifold associated to the final orbit. As optimization is carried out in the second phase only, overall optimality is lost. The same idea is replicated in a number of later works [17–20]. Alternatively, much higher initial orbits are chosen [10,21–24], though they are not practical for engineering applications.

In this Note, the complete optimal low-thrust GTO-to-halo transfer is solved for the first time. This result is achieved with an indirect approach and constant specific impulse engine. Thrust-to-mass ratios in agreement with currently available technology are considered. Some effective techniques are applied to cope with problem complexity. These methods involve solving the minimum-fuel, minimum-energy, and minimum-time problems [10,25], implementing energy-to-fuel homotopy [10,26–28], continuing the maximum thrust magnitude [10], computing the analytic Jacobians [9], and accurately detecting the switching points through a combination of Newton and bisection methods [29]. In the present approach, the solution structure is not prescribed (as in [16–18,20,30,31]), but rather it is found a posteriori, with low-thrust propulsion that is free to act everywhere; the final coast arc, recalling a stable manifold branch, is found automatically. The techniques presented in this Note are useful in practical cases where very low-thrust accelerations are used for long times in highly nonlinear vector fields.

The Note is organized as follows. In Sec. II, the dynamical model is presented, and the minimum-fuel, minimum-energy, and minimum-time problems are stated. In Sec. III, the analytical Jacobians for the minimum-energy and minimum-fuel problems are derived. In Sec. IV, the original, hybrid switching detection technique is presented, and details on practical implementation are given. The case study is solved in Sec. V, and critical analysis is conducted.

II. Statement of the Problem

A. Controlled Restricted Three-Body Problem

The circular restricted three-body problem studies the motion of a massless spacecraft P_3 under the gravitational field generated by two primaries, P_1 and P_2, of masses m_1 and m_2, respectively, which move in a circular motion due to their mutual interaction. The dynamics are written in a rotating frame with nondimensional units: the angular velocity of P_1, P_2, their distance, and the sum of their masses are all set to unity. The Earth–moon model is considered in this work, where $\mu = m_2/(m_1 + m_2) \simeq 0.012$. The Earth, of mass $(1-\mu)$, is located at $(-\mu, 0, 0)$, whereas the moon, of mass μ, is located at $(1-\mu, 0, 0)$; see [32] for details. When low-thrust propulsion is considered, it is convenient to write the equations of motions as [9]

$$\dot{\boldsymbol{x}} = \boldsymbol{f}(\boldsymbol{x}, \boldsymbol{\alpha}, u) \Rightarrow \begin{bmatrix} \dot{\boldsymbol{r}} \\ \dot{\boldsymbol{v}} \\ \dot{m} \end{bmatrix} = \begin{bmatrix} \boldsymbol{v} \\ \boldsymbol{g}(\boldsymbol{r}) + \boldsymbol{h}(\boldsymbol{v}) + uT_{\max}\boldsymbol{\alpha}/m \\ -uT_{\max}/c \end{bmatrix} \quad (1)$$

where $\boldsymbol{r} = [x, y, z]^\top$ and $\boldsymbol{v} = [v_x, v_y, v_z]^\top$ are the spacecraft position and velocity vectors, respectively; m denotes the spacecraft mass; $T_{\max}$ is the maximum thrust magnitude; and $c = I_{\mathrm{sp}} g_0$ represents the

Received 26 September 2014; revision received 30 December 2014; accepted for publication 8 January 2015; published online 12 March 2015.

*Ph.D. Candidate, School of Astronautics; buaa_zc@sa.buaa.edu.cn.
†Assistant Professor, Department of Aerospace Science and Technolgy; francesco.topputo@polimi.it.
‡Professor, Department of Aerospace Science and Technology; franco.bernelli@polimi.it.
§Professor, School of Astronautics; yszhao@buaa.edu.cn.

exhaust velocity (I_{sp} is the thruster specific impulse, and g_0 is the gravitational acceleration at the sea level). The control variables are the throttle factor, $u \in [0, 1]$, and the thrust direction unit vector $\boldsymbol{\alpha}$. The functions $\boldsymbol{g}(\boldsymbol{r})$ and $\boldsymbol{h}(\boldsymbol{v})$ are defined as [1,18]

$$\boldsymbol{g}(\boldsymbol{r}) = \begin{bmatrix} x - (1-\mu)(x+\mu)/r_1^3 - \mu(x+\mu-1)/r_2^3 \\ y - (1-\mu)y/r_1^3 - \mu y/r_2^3 \\ -(1-\mu)z/r_1^3 - \mu z/r_2^3 \end{bmatrix},$$

$$\boldsymbol{h}(\boldsymbol{v}) = \begin{bmatrix} 2v_y \\ -2v_x \\ 0 \end{bmatrix} \tag{2}$$

where r_1 and r_2 represent the distance of P_3 to the Earth and moon, respectively; i.e.,

$$r_1 = [(x+\mu)^2 + y^2 + z^2]^{1/2}, \quad r_2 = [(x+\mu-1)^2 + y^2 + z^2]^{1/2} \tag{3}$$

B. Construction of the Shooting Function

In minimum-fuel problems, a solution of Eq. (1) minimizes

$$J_f = \frac{T_{\max}}{c} \int_{t_i}^{t_f} u \, \mathrm{d}t \tag{4}$$

where t_i and t_f denote the initial and final times, respectively. In these problems, u is either zero or one [33]. This dichotomy causes discontinuities in the shooting function [28], and it poses severe restrictions on numerical methods. A smoothing technique, or homotopic approach, was introduced in [26] to relax the control profile and to enforce discontinuity in a gradual way [34]. It consists of using the objective function

$$J = \frac{T_{\max}}{c} \int_{t_i}^{t_f} [u - \varepsilon u(1-u)] \, \mathrm{d}t, \qquad \varepsilon \in [0, 1] \tag{5}$$

The minimum-energy problem ($\varepsilon = 1$) is solved first; the solution is then continued by decreasing ε until Eq. (4) is reached ($\varepsilon = 0$) [28]. In this work, optimal transfers between two given states [a point on the GTO ($\boldsymbol{r}_i, \boldsymbol{v}_i$), and a point on the L_1 halo ($\boldsymbol{r}_f, \boldsymbol{v}_f$)] are designed; therefore, the boundary conditions read

$$\begin{aligned} &\boldsymbol{r}(t_i) - \boldsymbol{r}_i = 0, \qquad \boldsymbol{v}(t_i) - \boldsymbol{v}_i = 0, \qquad m(t_i) - 1 = 0, \\ &\boldsymbol{r}(t_f) - \boldsymbol{r}_f = 0, \qquad \boldsymbol{v}(t_f) - \boldsymbol{v}_f = 0 \end{aligned} \tag{6}$$

where the initial mass is scaled to one, whereas the final mass is obviously unconstrained. The fixed terminal state formulation in Eq. (6), as opposed to that in [16,18,22–24], has been chosen to favor convergence. To vary the arrival point on the halo orbit, an outer loop can be implemented or a problem accounting for free terminal conditions can be stated.

The Hamiltonian of the problem is [35]

$$H = \boldsymbol{\lambda}_r \cdot \boldsymbol{v} + \boldsymbol{\lambda}_v \cdot \left[\boldsymbol{g}(\boldsymbol{r}) + \boldsymbol{h}(\boldsymbol{v}) + \frac{uT_{\max}}{m}\boldsymbol{\alpha} \right] - \lambda_m \frac{uT_{\max}}{c} + \frac{T_{\max}}{c}[u - \varepsilon u(1-u)] \tag{7}$$

where $\boldsymbol{\lambda} = [\boldsymbol{\lambda}_r, \boldsymbol{\lambda}_v, \lambda_m]^\top$ is the vector of costates, for which the dynamics are

$$\dot{\boldsymbol{\lambda}} = -\frac{\partial H}{\partial \boldsymbol{x}} \Rightarrow \begin{bmatrix} \dot{\boldsymbol{\lambda}}_r \\ \dot{\boldsymbol{\lambda}}_v \\ \dot{\lambda}_m \end{bmatrix} = \begin{bmatrix} -\boldsymbol{G}^\top \boldsymbol{\lambda}_v \\ -\boldsymbol{\lambda}_r - \boldsymbol{H}^\top \boldsymbol{\lambda}_v \\ uT_{\max}/m^2 \boldsymbol{\lambda}_v \cdot \boldsymbol{\alpha} \end{bmatrix} \tag{8}$$

with $\boldsymbol{G} = \partial \boldsymbol{g}(\boldsymbol{r})/\partial \boldsymbol{r}$ and $\boldsymbol{H} = \partial \boldsymbol{h}(\boldsymbol{v})/\partial \boldsymbol{v}$ (only nonzero elements listed):

$$\begin{aligned} &G_{1,1} = 1 - (1-\mu)/r_1^3 + 3(1-\mu)(x+\mu)^2/r_1^5 - \mu/r_2^3 + 3\mu(x+\mu-1)^2/r_2^5, \\ &G_{2,2} = 1 - (1-\mu)/r_1^3 + 3(1-\mu)y^2/r_1^5 - \mu/r_2^3 + 3\mu y^2/r_2^5, \\ &G_{3,3} = -(1-\mu)/r_1^3 + 3(1-\mu)z^2/r_1^5 - \mu/r_2^3 + 3\mu z^2/r_2^5, \\ &G_{1,2} = G_{2,1} = 3(1-\mu)(x+\mu)y/r_1^5 + 3\mu(x+\mu-1)y/r_2^5, \\ &G_{1,3} = G_{3,1} = 3(1-\mu)(x+\mu)z/r_1^5 + 3\mu(x+\mu-1)z/r_2^5, \\ &G_{2,3} = G_{3,2} = 3(1-\mu)yz/r_1^5 + 3\mu yz/r_2^5, \; H_{1,2} = -H_{2,1} = 2 \end{aligned}$$

Due to Eq. (6), the boundary conditions for the costates are all unknown except for λ_m. As the final mass is free, its associated costate must be zero at t_f [35], i.e.,

$$\lambda_m(t_f) = 0 \tag{9}$$

The conditions on the control variables u and $\boldsymbol{\alpha}$ are derived by applying the Pontryagin maximum principle (PMP) [36], which states that the Hamiltonian is minimized along an optimal trajectory. Since $uT_{\max}/m \geq 0$ in Eq. (7), then the optimal thrust direction is [37]

$$\boldsymbol{\alpha}^* = -\boldsymbol{\lambda}_v/\lambda_v \tag{10}$$

Substituting Eq. (10) into Eq. (7) yields

$$H = \boldsymbol{\lambda}_r \cdot \boldsymbol{v} + \boldsymbol{\lambda}_v \cdot [\boldsymbol{g}(\boldsymbol{r}) + \boldsymbol{h}(\boldsymbol{v})] + \frac{uT_{\max}}{c}(S - \varepsilon + \varepsilon u) \tag{11}$$

where a switching function S is defined as

$$S = -\lambda_v \frac{c}{m} - \lambda_m + 1 \tag{12}$$

along with its first derivative

$$\dot{S} = \frac{c}{m} \frac{(-\boldsymbol{\lambda}_r - \boldsymbol{H}^\top \boldsymbol{\lambda}_v) \cdot \boldsymbol{\lambda}_v}{\lambda_v} \tag{13}$$

The throttle factor u is the only decision variable in Eq. (11). Its value can be related to $\boldsymbol{x}$ and $\boldsymbol{\lambda}$ by applying it again the PMP. The optimal value u^* can be stated in terms of S through

$$\begin{aligned} &u^* = 0 \quad \text{if } S > \varepsilon \\ &u^* = (\varepsilon - S)/2\varepsilon \quad \text{if } -\varepsilon \leq S \leq \varepsilon \\ &u^* = 1 \quad \text{if } S < -\varepsilon \end{aligned} \tag{14}$$

Note that, in minimum-fuel problems ($\varepsilon = 0$), the magnitude of u^* depends only upon the sign of S, and a bang–bang profile is generated.

Once the optimal control variables $\boldsymbol{\alpha}^*$ and u^* are determined as functions of the states and costates, through Eqs. (10) and (14), the motion can be integrated implicitly with dynamics

$$\dot{\boldsymbol{y}} = \boldsymbol{F}(\boldsymbol{y}) \Rightarrow \begin{bmatrix} \dot{\boldsymbol{r}} \\ \dot{\boldsymbol{v}} \\ \dot{m} \\ \dot{\boldsymbol{\lambda}}_r \\ \dot{\boldsymbol{\lambda}}_v \\ \dot{\lambda}_m \end{bmatrix} = \begin{bmatrix} \boldsymbol{v} \\ \boldsymbol{g}(\boldsymbol{r}) + \boldsymbol{h}(\boldsymbol{v}) - (\boldsymbol{\lambda}_v/\lambda_v)uT_{\max}/m \\ -uT_{\max}/c \\ -\boldsymbol{G}^\top \boldsymbol{\lambda}_v \\ -\boldsymbol{\lambda}_r - \boldsymbol{H}^\top \boldsymbol{\lambda}_v \\ -\lambda_v uT_{\max}/m^2 \end{bmatrix} \tag{15}$$

where $\boldsymbol{y} = [\boldsymbol{x}, \boldsymbol{\lambda}]^\top$ is a 14-dimensional canonical variable [9]. A two-point boundary value problem is defined by Eq. (15) together with the boundary conditions [Eqs. (6) and (9)]. If the initial costate vector $\boldsymbol{\lambda}_i$ was given, one could integrate Eq. (15) [with u as in Eq. (14)] and check if the final conditions are verified. In the likely case in which these are not met, $\boldsymbol{\lambda}_i$ can be adjusted based on first-order information. This scheme is the essence of the shooting procedure.

Remark 1: Let $[\boldsymbol{x}(t), \boldsymbol{\lambda}(t)]^\top = \boldsymbol{\varphi}([\boldsymbol{x}_i, \boldsymbol{\lambda}_i]^\top, t_i, t)$ be the solution of Eq. (15) integrated from $[\boldsymbol{x}_i, \boldsymbol{\lambda}_i]^\top$, from the initial time t_i to a generic time t. The optimization problem is stated as follows:

$$\text{Find } \boldsymbol{\lambda}_i \text{ such that} [\boldsymbol{x}(t_f), \boldsymbol{\lambda}(t_f)]^\top = \boldsymbol{\varphi}([\boldsymbol{x}_i, \boldsymbol{\lambda}_i]^\top, t_i, t_f) \text{ satisfies } \begin{cases} \boldsymbol{r}(t_f) - \boldsymbol{r}_f = 0 \\ \boldsymbol{v}(t_f) - \boldsymbol{v}_f = 0 \\ \lambda_m(t_f) = 0 \end{cases} \tag{16}$$

More synthetically, the problem is to find $\boldsymbol{\lambda}_i$ such that $\boldsymbol{Z}(\boldsymbol{\lambda}_i) = 0$, where $\boldsymbol{Z}(\boldsymbol{\lambda})$, or the shooting function, is the seven-dimensional vector-valued function given by the final boundary conditions [Eq. (16)]. As finding the zeros of $\boldsymbol{Z}(\boldsymbol{\lambda})$ is not trivial, a number of techniques have to be implemented.

C. Minimum-Time Problem

A minimum-time step has to be solved to infer the minimum possible transfer time $t_{f_{\min}}$ for each $T_{\max}$; see [10]. The minimum-fuel problem [Eq. (16)] has to be solved then for $t_f \geq t_{f_{\min}}$. The performance index of minimum-time problems is

$$J_t = \int_{t_i}^{t_f} 1 \, \mathrm{d}t$$

therefore, the Hamiltonian reads

$$H_t = \boldsymbol{\lambda}_r \cdot \boldsymbol{v} + \boldsymbol{\lambda}_v \cdot \left[\boldsymbol{g}(\boldsymbol{r}) + \boldsymbol{h}(\boldsymbol{v}) + \frac{uT_{\max}}{m} \boldsymbol{\alpha} \right] - \lambda_m \frac{uT_{\max}}{c} + 1 \tag{17}$$

Applying the PMP to Eq. (17) yields

$$u^* = 0 \quad \text{if } S_t > 0 \quad u^* \in [0, 1] \quad \text{if } S_t = 0 \quad u^* = 1 \quad \text{if } S_t < 0 \tag{18}$$

where the minimum-time switching function is

$$S_t = -\lambda_v \frac{c}{m} - \lambda_m \tag{19}$$

When the final time is free, the transversality condition sets $H_t(t_f)$ to zero [25].

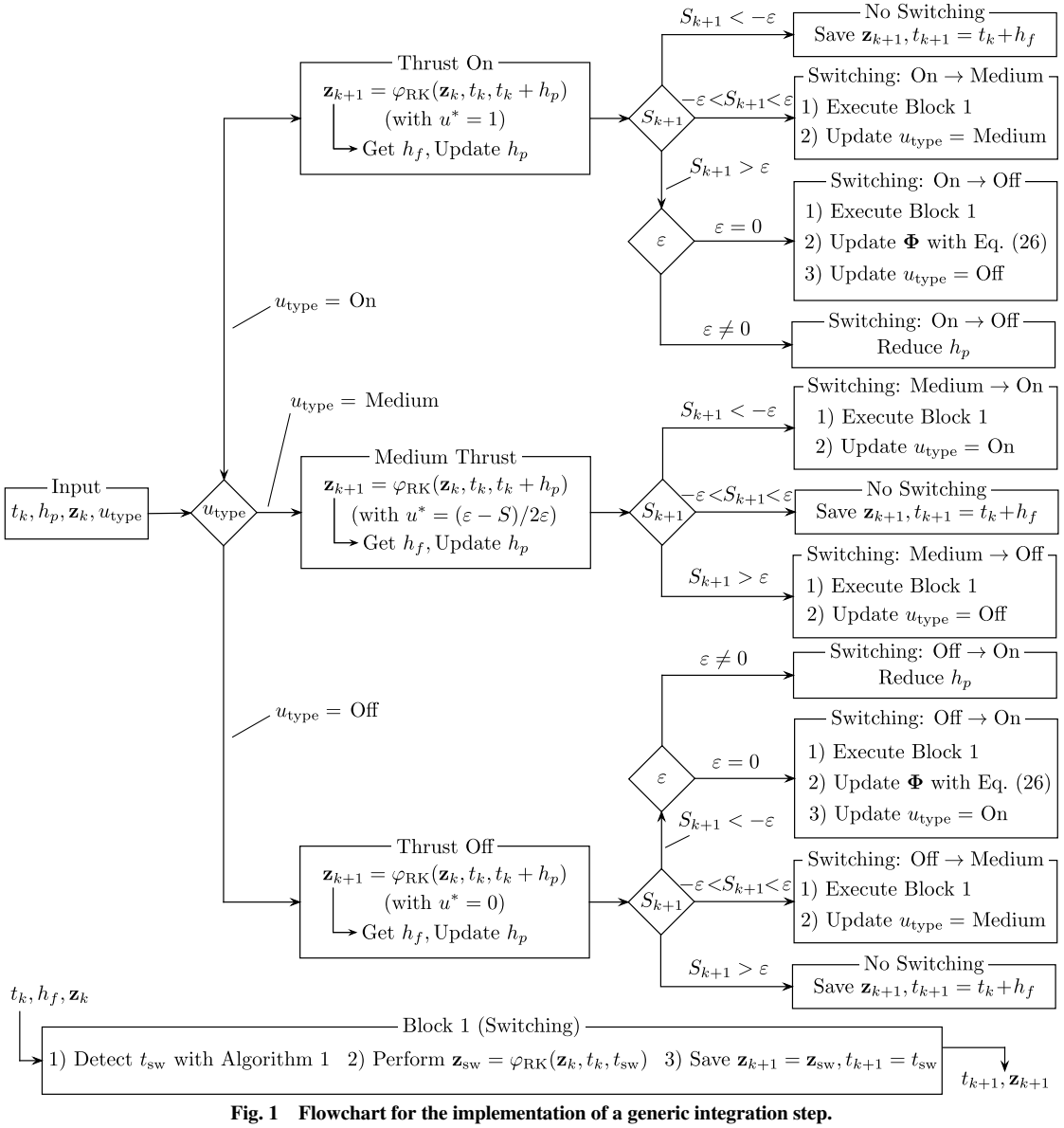

Fig. 1 Flowchart for the implementation of a generic integration step.

Remark 2: The minimum-time problem is stated as follows:

$$\text{Find } (\boldsymbol{\lambda}_i, t_f) \text{ such that } [\boldsymbol{x}(t_f), \boldsymbol{\lambda}(t_f)]^\top = \boldsymbol{\varphi}([\boldsymbol{x}_i, \boldsymbol{\lambda}_i]^\top, t_i, t_f) \text{ satisfies } \begin{cases} \boldsymbol{r}(t_f) - \boldsymbol{r}_f = 0 \\ \boldsymbol{v}(t_f) - \boldsymbol{v}_f = 0 \\ \lambda_m(t_f) = 0 \\ H_t(t_f) = 0 \end{cases} \tag{20}$$

III. Analytic Derivatives

To increase the accuracy and robustness of the shooting procedure, analytic derivatives are provided. In particular, the state transition matrix (STM) of Eq. (15), $\boldsymbol{\Phi}(t_i, t) = \mathrm{d}\boldsymbol{\varphi}(\boldsymbol{y}, t_i, t)/\mathrm{d}\boldsymbol{y}$, is derived. The STM maps small variations in the initial condition $\delta \boldsymbol{y}_i$ over $t_i \to t$, i.e., $\delta \boldsymbol{y}(t) = \boldsymbol{\Phi}(t_i, t)\delta \boldsymbol{y}(t_i)$. The STM is subject to the variational equation

$$\dot{\boldsymbol{\Phi}}(t_i, t) = D_{\boldsymbol{y}}\boldsymbol{F}\boldsymbol{\Phi}(t_i, t), \qquad \boldsymbol{\Phi}(t_i, t_i) = \boldsymbol{I}_{14\times 14} \tag{21}$$

where $D_{\boldsymbol{y}}\boldsymbol{F}$, the Jacobian of $\boldsymbol{F}(\boldsymbol{y})$ in Eq. (15), has two different expressions: A) for $u^* = 0$ or $u^* = 1$, and B) for $u^* = (\varepsilon - S)/2$ [see Eqs. (12), (14), and (15)], i.e.,

$$D_{\boldsymbol{y}}\boldsymbol{F}^{(A)} = \left[\begin{array}{ccc:ccc} 0 & I & 0 & 0 & 0 & 0 \\ G & H & \frac{\lambda_v}{\lambda_v}\frac{uT_{\max}}{m^2} & 0 & -\frac{uT_{\max}}{m}\left(\frac{I}{\lambda_v} - \frac{\lambda_v \lambda_v^\top}{\lambda_v^3}\right) & 0 \\ 0 & 0 & 0 & 0 & 0 & 0 \\ \hdashline -\frac{\partial(G^\top \lambda_v)}{\partial r} & 0 & 0 & 0 & -G^\top & 0 \\ 0 & 0 & 0 & -I & -H^\top & 0 \\ 0 & 0 & \frac{2\lambda_v u T_{\max}}{m^3} & 0 & -\frac{\lambda_v^\top}{\lambda_v}\frac{uT_{\max}}{m^2} & 0 \end{array}\right] \tag{22}$$

$$D_{\boldsymbol{y}}\boldsymbol{F}^{(B)} = \left[\begin{array}{ccc:ccc} 0 & I & 0 & 0 & 0 & 0 \\ G & H & \Omega_1 & 0 & \Omega_2 & \Omega_3 \\ 0 & 0 & \Omega_4 & 0 & \Omega_5 & \Omega_6 \\ \hdashline -\frac{\partial(G^\top \lambda_v)}{\partial r} & 0 & 0 & 0 & -G^\top & 0 \\ 0 & 0 & 0 & -I & -H^\top & 0 \\ 0 & 0 & \Omega_7 & 0 & \Omega_8 & \Omega_9 \end{array}\right] \tag{23}$$

where

$$\boldsymbol{\Omega}_1 = \frac{\lambda_v}{\lambda_v}\frac{uT_{\max}}{m^2} + \frac{\lambda_v c T_{\max}}{2\varepsilon m^3} \qquad \boldsymbol{\Omega}_2 = -\frac{\lambda_v \lambda_v^\top}{\lambda_v^2}\frac{cT_{\max}}{2\varepsilon m^2} - \frac{uT_{\max}}{m}\left(\frac{\boldsymbol{I}}{\lambda_v} - \frac{\lambda_v \lambda_v^\top}{\lambda_v^3}\right) \qquad \boldsymbol{\Omega}_3 = -\frac{\lambda_v}{\lambda_v}\frac{T_{\max}}{2\varepsilon m}$$

$$\boldsymbol{\Omega}_4 = \frac{\lambda_v T_{\max}}{2\varepsilon m^2} \qquad \boldsymbol{\Omega}_5 = -\frac{\lambda_v^\top}{\lambda_v}\frac{T_{\max}}{2\varepsilon m} \qquad \boldsymbol{\Omega}_6 = -\frac{T_{\max}}{2\varepsilon c}$$

$$\boldsymbol{\Omega}_7 = \frac{2\lambda_v u T_{\max}}{m^3} + \frac{\lambda_v^2 c T_{\max}}{2\varepsilon m^4} \qquad \boldsymbol{\Omega}_8 = -\frac{\lambda_v^\top}{\lambda_v}\frac{uT_{\max}}{m^2} - \frac{\lambda_v^\top c T_{\max}}{2\varepsilon m^3}$$

$$\boldsymbol{\Omega}_9 = -\frac{\lambda_v T_{\max}}{2\varepsilon m^2}$$

Note that Eq. (21) is equivalent to 196 first-order differential equations for the elements of $\boldsymbol{\Phi}(t_i, t)$; it requires $D_{\boldsymbol{y}}\boldsymbol{F}$ to be evaluated along $\boldsymbol{y}(t)$; therefore, Eqs. (15) and (21) have to be integrated simultaneously. Let $\boldsymbol{z}$ be a vector containing $\boldsymbol{y}$ and columns of $\boldsymbol{\Phi}$; its first-order variation is

$$\dot{\boldsymbol{z}} = \mathcal{F}(\boldsymbol{z}) \Rightarrow \begin{bmatrix} \dot{\boldsymbol{y}} \\ \mathrm{vec}(\dot{\boldsymbol{\Phi}}) \end{bmatrix} = \begin{bmatrix} \boldsymbol{F}(\boldsymbol{y}) \\ \mathrm{vec}(D_{\boldsymbol{y}}\boldsymbol{F}\boldsymbol{\Phi}) \end{bmatrix} \tag{24}$$

where "vec" is an operator that converts the matrix into a column vector. Equation (24) yields 210 nonlinear differential equations. It is worth mentioning that $\boldsymbol{\Phi}(t_i, t)$ only maps states along a continuous orbit. If at time t_j there is a "bang–bang" switching point, a discontinuity arises, and the STM across such a discontinuity, $\boldsymbol{\Psi}(t_j)$, has to be determined. This STM can be computed as [9]

Algorithm 1 Switching time determination

1: Initialize $t_{\mathrm{sw}} = t_k$.
2: Compute $t_{\mathrm{sw}} = t_{\mathrm{sw}} - f(t_{\mathrm{sw}})/\dot{S}(t_{\mathrm{sw}})$.
3: Perform $\boldsymbol{y}(t_{\mathrm{sw}}) = \boldsymbol{\varphi}_{\mathrm{RK}}(\boldsymbol{y}_k, t_k, t_{\mathrm{sw}})$.
4: Evaluate $f(t_{\mathrm{sw}})$ and $\dot{S}(t_{\mathrm{sw}})$ with $\boldsymbol{y}(t_{\mathrm{sw}})$.
5: Repeat steps ii)–iv) until $f(t_{\mathrm{sw}}) <$ tol.

In case $f(t_{\mathrm{sw}}) >$ tol or $t_{\mathrm{sw}} < t_k$ or $t_{\mathrm{sw}} > t_{k+1}$, execute a bisection method within (t_k, t_{k+1}).

$$\Psi(t_j) = \frac{\partial \boldsymbol{y}(t_j^+)}{\partial \boldsymbol{y}(t_j^-)} = \boldsymbol{I}_{14\times 14} + (\dot{\boldsymbol{y}}|_{t_j^+} - \dot{\boldsymbol{y}}|_{t_j^-})\left(\frac{\partial S}{\partial \boldsymbol{y}}\frac{1}{\dot{S}}\right)\Bigg|_{t_j^-} \tag{25}$$

where t_j^- and t_j^+ represent the times immediately before and after the discontinuity. In the likely case in which there are N bang–bang points at times $t_1, \ldots, t_N$, the composite STM is given by [9]

$$\boldsymbol{\Phi}(t_f, t_i) = \boldsymbol{\Phi}(t_f, t_N^+)\boldsymbol{\Psi}(t_N)\boldsymbol{\Phi}(t_N^-, t_{N-1}^+)\boldsymbol{\Psi}(t_{N-1})\ldots\boldsymbol{\Phi}(t_2^-, t_1^+)$$
$$\boldsymbol{\Psi}(t_1)\boldsymbol{\Phi}(t_1^-, t_i) = \frac{\partial \boldsymbol{y}(t_f)}{\partial \boldsymbol{y}(t_i)} \tag{26}$$

IV. Switching Detection Techniques

It has been mentioned that the right-hand side of Eq. (15) is discontinuous. When numerical integration is performed, discontinuities cause the integration error to accumulate about the switching

Table 1 Physical constants

Physical constant	Value
Mass parameter μ	$1.21506683 \times 10^{-2}$
Gravitational field g_0	9.80665 m/s^2
Length unit (LU)	3.84405000×10^5 km
Time unit	3.75676967×10^5 s
Speed unit (VU)	1.02323281 km/s
Mass unit	1500 kg

Table 2 Boundary conditions

Boundary condition	Values
Initial position vector	$\boldsymbol{r}_i = [-0.019488511458668, -0.016033479812051, 0]^\top$ LU
Initial velocity vector	$\boldsymbol{v}_i = [8.918881923678198, -4.081793688818725, 0]^\top$ VU
Final position vector	$\boldsymbol{r}_f = [0.823385182067467, 0, -0.022277556273235]^\top$ LU
Final velocity vector	$\boldsymbol{v}_f = [0, 0.134184170262437, 0]^\top$ VU

Table 3 Minimum-time solutions computed

$T_{\max}$, N	$T_{\max}/m_i$, m/s^2	$t_{f_{\min}}$, days	m_f	Δv, km/s
10	6.6667×10^{-3}	7.8549	0.8462	4.8015
9	6.0000×10^{-3}	8.6861	0.8469	4.7777
8	5.3333×10^{-3}	9.6522	0.8488	4.7133
7	4.6667×10^{-3}	10.8133	0.8518	4.6119
6	4.0000×10^{-3}	12.6278	0.8516	4.6186
5	3.3333×10^{-3}	12.9634	0.8730	3.9050
4	2.6667×10^{-3}	16.0510	0.8742	3.8655
3	2.0000×10^{-3}	21.1363	0.8758	3.8130
2	1.3333×10^{-3}	29.1512	0.8858	3.4865
1	6.6667×10^{-4}	56.2458	0.8898	3.3570
0.9	6.0000×10^{-4}	59.8376	0.8945	3.2055
0.8	5.3333×10^{-4}	64.6165	0.8987	3.0708
0.7	4.6667×10^{-4}	80.2242	0.8900	3.3505
0.6	4.0000×10^{-4}	87.6674	0.8970	3.1253
0.5	3.3333×10^{-4}	112.0327	0.8903	3.3408
0.4	2.6667×10^{-4}	138.4519	0.8915	3.3021
0.3	2.0000×10^{-4}	171.6254	0.8991	3.0580

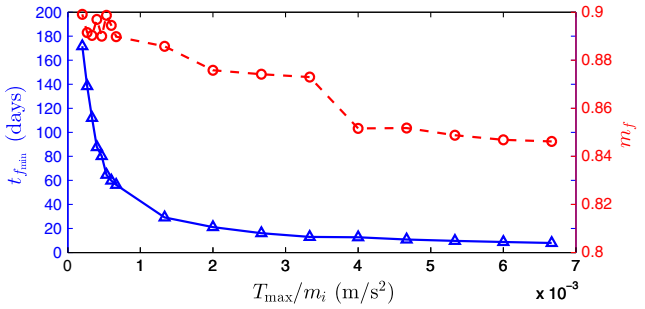

Fig. 2 Minimum transfer time $t_{f_{min}}$ and final mass ratio m_f versus thrust acceleration, T_{max}/m_i, in minimum-time solutions.

points if these are not explicitly determined, which in turn threatens the entire shooting process. A hybrid switching detection technique combined with a variable-step integration has been implemented to precisely detect the switching times. Let t_k and t_{k+1} be two consecutive integration steps, and let $\boldsymbol{y}_k = \boldsymbol{y}(t_k)$ and $\boldsymbol{y}_{k+1} = \boldsymbol{y}(t_{k+1})$. These states are linked through $\boldsymbol{y}_{k+1} = \boldsymbol{\varphi}_{RK}(\boldsymbol{y}_k, t_k, t_{k+1})$, where $\boldsymbol{\varphi}_{RK}$ is the numerical integration map. Also, let t_{sw} be the switching time, and $S_k = S(\boldsymbol{y}(t_k))$ and $S_{k+1} = S(\boldsymbol{y}(t_{k+1}))$, as per the switching function [Eq. (12)]. With reference to Eq. (14), suppose that $S_k > \varepsilon$ and $-\varepsilon < S_{k+1} < \varepsilon$; extending the analysis to the other cases in Eq. (14) is straightforward. The focus is to determine the switching time t_{sw}, $t_{sw} \in (t_k, t_{k+1})$, which zeroes $f(t_{sw}) = S(t_{sw}) - \varepsilon$.

The hybrid switching detection procedure developed is made up of two steps. First, the Newton method is implemented because of its high efficiency; in general, only four to five iterations are needed to reach machine precision (i.e., 10^{-15}). The first guess is set to t_k, and the analytic derivative in Eq. (13) is used. In case the Newton method fails or converges to solutions outside of the searching interval (t_k, t_{k+1}), a bisection procedure is executed. The latter is slower but more robust.

The low-thrust trajectory optimization problem has been implemented in a numerical framework. The seventh/eighth-order Runge–Kutta scheme, with relative and absolute tolerances set to 10^{-14}, has been used to integrate Eqs. (15) and (21) [or, equivalently, Eq. (24)], with the implicit optimal thrusting strategy in Eq. (14). The implementation of a generic integration step is outlined in Fig. 1.

The input required to execute an integration step are 1) t_k, the initial integration time; 2) h_p, the step size predicted at a previous integration step (a value is guessed at first step); 3) $\boldsymbol{z}_k$, the 210-dimensional composite state at t_k [state and costate, $\boldsymbol{y}_k$, and the elements of $\boldsymbol{\Phi}(t_i, t_k)$; see Eq. (24)]; and 4) u_{type}, the logical thrust type at the previous integration step, i.e., on, medium, or off according to Eq. (14) (only on or off in minimum-fuel problems). According to u_{type}, the flow is redirected to one of the three integration blocks in Fig. 1, where a prediction on $\boldsymbol{z}_{k+1}$ is made: $\boldsymbol{z}_{k+1} = \boldsymbol{\varphi}_{RK}(\boldsymbol{z}_k, t_k, t_k + h_p)$. Note that $\boldsymbol{z}_{k+1}$ is the composite state at time $t_{k+1} = t_k + h_f$, where h_f is the step size corrected during the Runge–Kutta integration, which also updates the value of h_p for the subsequent integration. A correction is then made according to the value of the switching function S_{k+1}. The branch tagged with "Thrust On" is analyzed for brevity. According to the relations [Eq. (14)], if $S_{k+1} < -\varepsilon$, the thrusting strategy is not changed over $[t_k, t_{k+1}]$; therefore, t_{k+1} and $\boldsymbol{z}_{k+1}$ are saved. When $-\varepsilon < S_{k+1} < \varepsilon$, a switching (from on to medium) occurs in $[t_k, t_{k+1}]$. In this case, the switching time t_{sw} as well as the state at the switching point $\boldsymbol{z}_{sw}$ are detected with Algorithm 1, and u_{type} is updated (see "Block 1" at the bottom of Fig. 1). In the case of $S_{k+1} > \varepsilon$, two options are possible: 1) in the minimum-energy problem ($\varepsilon \neq 0$), jumping from thrust on to off is not possible, and therefore the step size has to be reduced and the process must be repeated; and

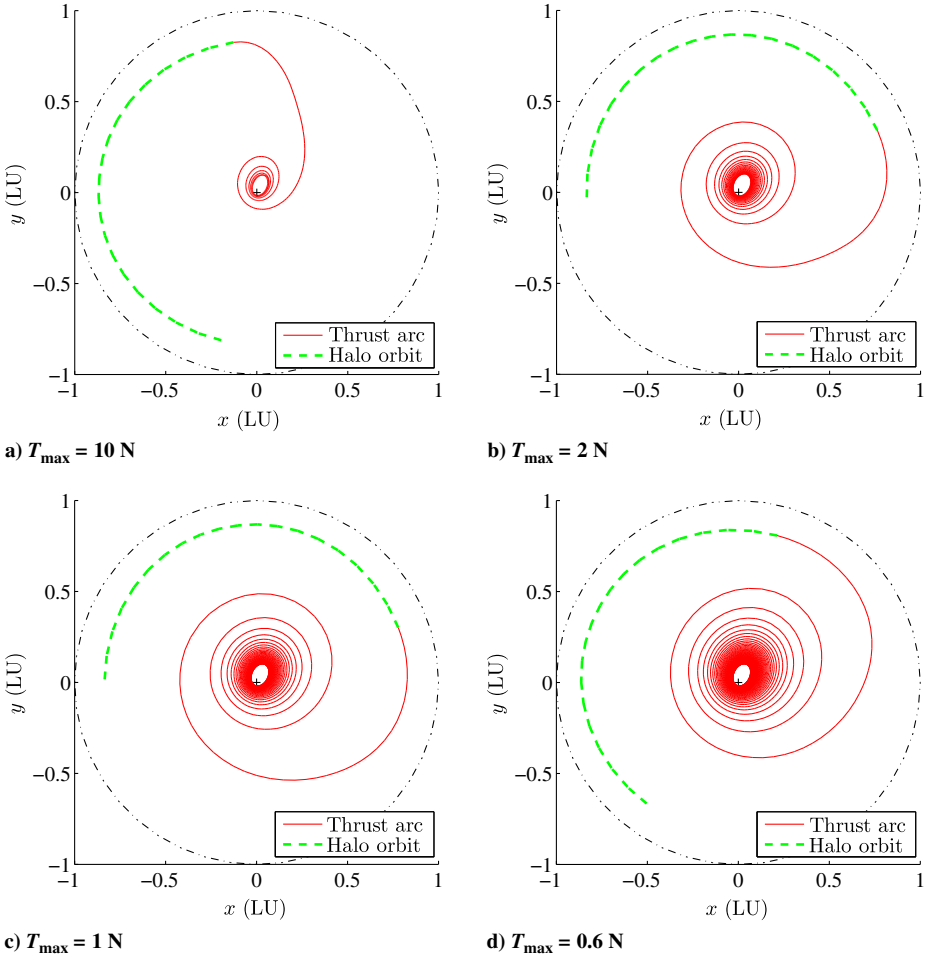

a) T_{max} = 10 N **b) T_{max} = 2 N**

c) T_{max} = 1 N **d) T_{max} = 0.6 N**

Fig. 3 Minimum-time trajectories for different values of T_{max}; Earth-centered inertial frame.

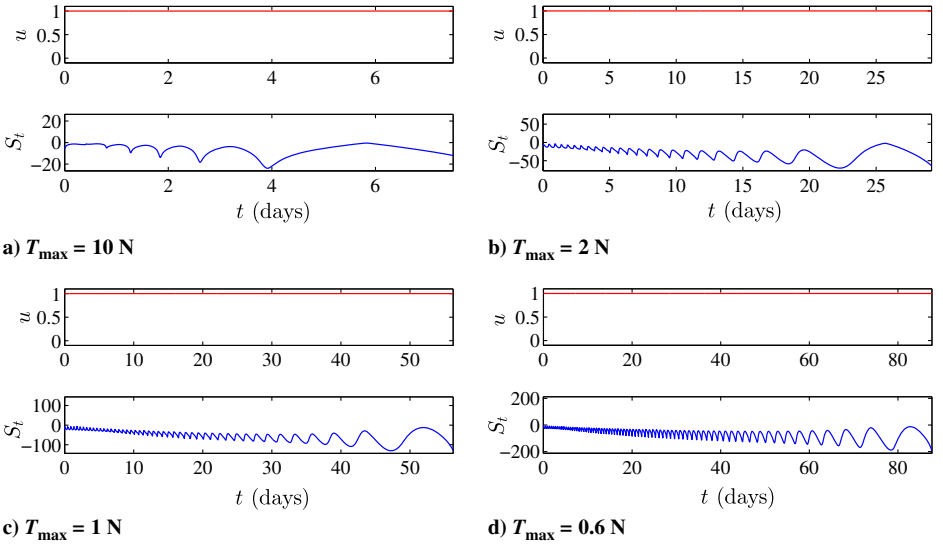

a) $T_{\max}$ = 10 N b) $T_{\max}$ = 2 N

c) $T_{\max}$ = 1 N d) $T_{\max}$ = 0.6 N

Fig. 4 Throttle factor u and switching function S_t profiles in minimum-time solutions.

2) in the minimum-fuel problem ($\varepsilon = 0$), the switching time is detected, along with the state at the switching point, and the control type is updated. In the latter case, the STM is updated by considering the control discontinuity as in Eq. (25).

V. Simulations and Results

The case study is a low-thrust transfer from a GTO to a L_1 halo orbit in the Earth–moon system. The GTO has periapsis and apoapsis altitudes of $h_p = 400$ km and $h_a = 35,864$ km, respectively. The specific impulse is 3000 s, and the initial satellite mass is 1500 kg. The transfer begins at periapsis. From this point on, the low-thrust propulsion is used to increase the energy until a particular point on the halo orbit is targeted. Numerical experiments show that varying the target point has negligible impact over the total cost of the transfer. This orbit has an out-of-plane amplitude of 8000 km, and it is consistent with [16–18,20]. Table 1 summarizes the parameters used in this work. The basis for distance, time, velocity, and mass units are the Earth–moon distance, the inverse of their orbital angular velocity, the lunar circular speed, and the initial spacecraft mass, respectively. Table 2 reports the initial and final conditions.

A. Minimum-Time Solutions

A minimum-time step is necessary to infer the minimum time required to accomplish the transfer $t_{f_{\min}}$ for a given maximum thrust $T_{\max}$. Once $t_{f_{\min}}$ is known, the subsequent energy-to-fuel optimization is formulated with a fixed final time t_f satisfying $t_f \geq t_{f_{\min}}$ at each $T_{\max}$. A continuation on $T_{\max}$ is performed. That is, at iteration k, problem (20) is solved for a given value of thrust, and the pair $(\boldsymbol{\lambda}_i^{[k]}, t_{f_{\min}}^{[k]})$ is used as a first-guess solution in iteration $k+1$, with decreased $T_{\max}$ (see Sec. II.C). Solutions with $T_{\max}$ ranging from 10 N down to 0.3 N have been achieved, with transfer times that increase accordingly from 7.8 to 171.6 days. The results, in terms of $t_{f_{\min}}$ and m_f are reported in Table 3 for different $T_{\max}$, and their trend versus the initial thrust-to-mass ratio $T_{\max}/m_i$ is drawn in Fig. 2. The transfer trajectories corresponding to $T_{\max}$ of 10, 2, 1, and 0.6 N are reported in Fig. 3 in the Earth-centered frame. The throttle factor and switching function trends are instead reported in Fig. 4. In these solutions, the thrust is always on; i.e., S_t in Eq. (19) is always negative, which triggers the last condition [Eq. (18)].

B. Minimum-Fuel Solutions

Minimum-fuel solutions are computed with a two-step continuation:

1) The minimum-energy problem ($\varepsilon = 1$) is solved iteratively with decreasing $T_{\max}$.

2) Once a low level of thrust is reached, ε is decreased until the minimum-fuel problem ($\varepsilon = 0$) is reached.

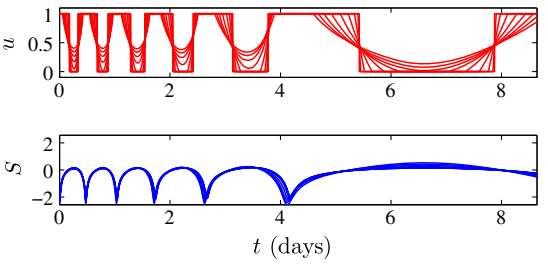

Fig. 5 Throttle factor u and switching function S for $T_{\max} = 10$ N.

Figure 5 reports the thrust profile and switching function for the 10 steps needed to switch from minimum-energy to minimum-fuel, $T_{\max} = 10$ N. In this example, the continuation law is $\varepsilon_j = (j^2 - 1)/(N^2 - 1)$, with $j = 10, 9, \ldots, 2, 1$ and $N = 10$. The ability of the process in smoothing the thrust profile gradually is evident. For each $T_{\max}$, the transfer time is chosen such that $t_f = c_{t_f} \times t_{f\,\min}$, where c_{t_f} is a coefficient selected manually. In step 2, varying c_{t_f} is a practical method to overcome convergence problems. The sensitivity of the final mass with respect to c_{t_f} is not considered.

For the sake of completeness, both minimum-energy and minimum-fuel solutions are reported for different values of $T_{\max}$ in Table 4. As expected, for each $T_{\max}$, minimum-fuel solutions use less propellant than minimum-energy ones. The solution with $T_{\max} = 0.6$ N has a thrust-to-mass ratio of 4×10^{-4} m/s^2, which is consistent with the current state of the art, and it agrees with [16–25]. This solution takes 140 days and needs just 8.5% of the propellant mass fraction. Compared to the analogous minimum-time solution, this means saving

Table 4 Solutions to minimum-energy ($\varepsilon = 1$) and minimum-fuel ($\varepsilon = 0$) cases, for different $T_{\max}$

$T_{\max}$, N	$T_{\max}/m_i$, m/s^2	c_{t_f}	t_f, days	m_f ($\varepsilon = 1$)	m_f ($\varepsilon = 0$)
10	6.6667×10^{-3}	1.1	8.6404	0.9034	0.9105
9	6.0000×10^{-3}	1.1	9.5548	0.9016	0.9103
8	5.3333×10^{-3}	1.1	10.6174	0.9003	0.9090
7	4.6667×10^{-3}	1.1	11.8946	0.8988	0.9072
6	4.0000×10^{-3}	1.2	15.1533	0.9009	0.9092
5	3.3333×10^{-3}	1.3	16.8524	0.8964	0.9053
4	2.6667×10^{-3}	1.3	20.8663	0.8936	0.9015
3	2.0000×10^{-3}	1.3	27.4773	0.8992	0.9088
2	1.3333×10^{-3}	1.3	37.8965	0.9091	0.9146
1	6.6667×10^{-4}	1.5	84.3688	0.9038	0.9131
0.6	4.0000×10^{-4}	1.6	140.2678	0.9069	0.9150

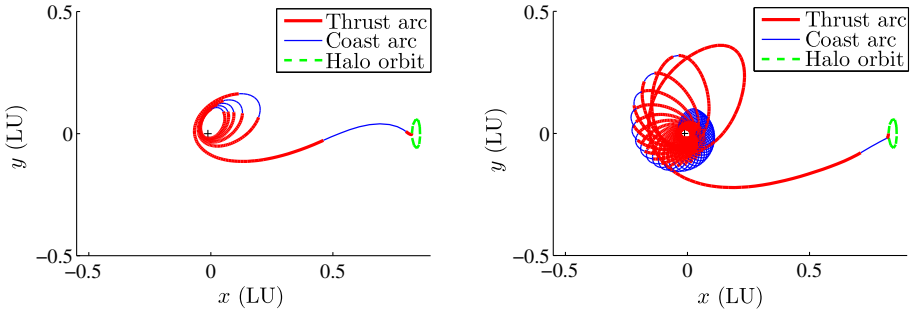

a) $T_{\max}$ = 10 N, c_{t_f} = 1.1

b) $T_{\max}$ = 2 N, c_{t_f} = 1.3

c) $T_{\max}$ = 1 N, c_{t_f} = 1.5

d) $T_{\max}$ = 0.6 N, c_{t_f} = 1.6

Fig. 6 Minimum-fuel trajectories for different values of $T_{\max}$; rotating frame.

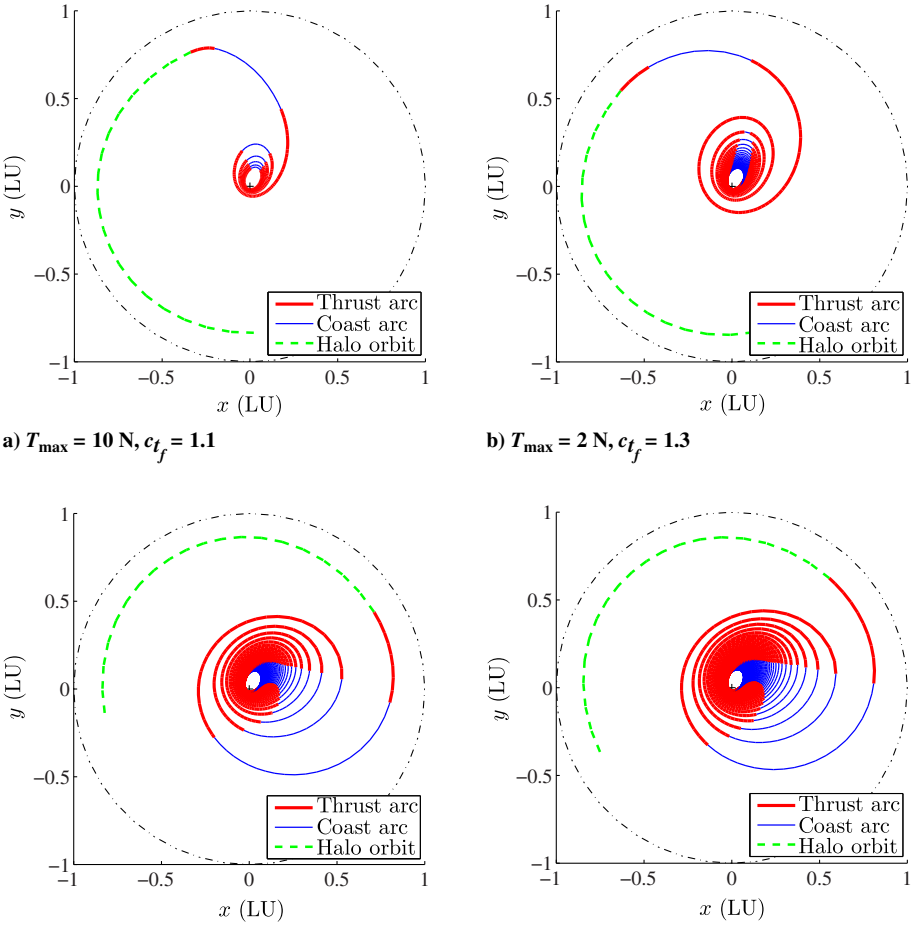

a) $T_{\max}$ = 10 N, c_{t_f} = 1.1

b) $T_{\max}$ = 2 N, c_{t_f} = 1.3

c) $T_{\max}$ = 1 N, c_{t_f} = 1.5

d) $T_{\max}$ = 0.6 N, c_{t_f} = 1.6

Fig. 7 Minimum-fuel trajectories for different values of $T_{\max}$; Earth-centered inertial frame.

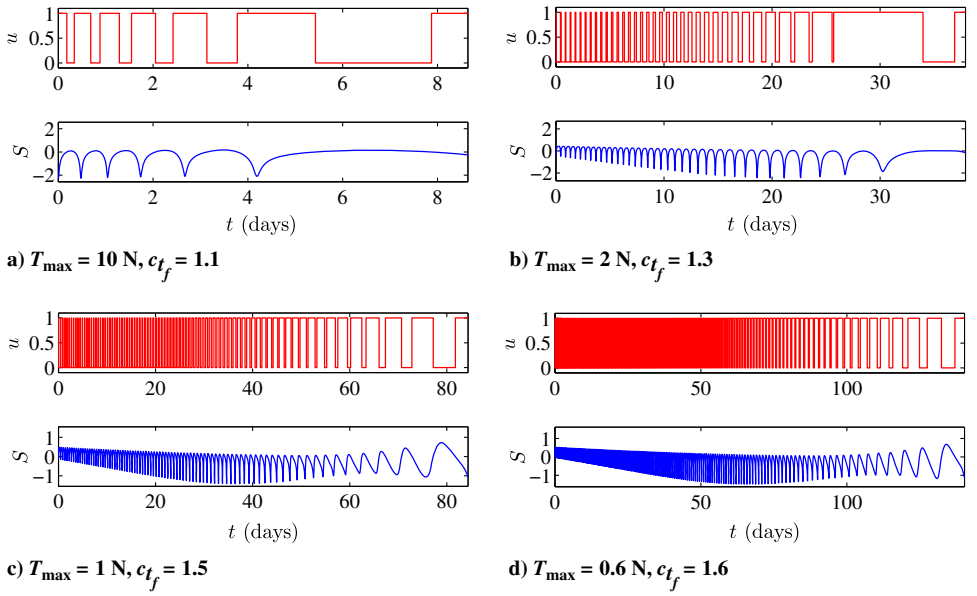

Fig. 8 Throttle factor u and switching function S profiles in minimum-fuel solutions.

27 kg of propellant at the cost of spending an additional 53 days of flight time.

Four sample minimum-fuel transfer trajectories are shown in Fig. 6 (rotating frame) and Fig. 7 (inertial frame). In both figures, the thick and thin lines indicate thrust and coast arcs, respectively. It can be seen that, in the minimum-fuel solutions, the thruster is on duty across the periapses (see Fig. 7). The algorithm is also capable of exploiting the stable structure associated to the halo orbit: all solutions foresee a final coast arc, which injects the spacecraft toward L_1 (the very final short thrust arc is the orbit injection maneuver; see Fig. 6). The long-duration multispiral features of the low-thrust solutions can be appreciated in Figs. 6d and 7d.

The trends for u and S corresponding to the solutions in Figs. 6 and 7 are reported in Fig. 8. The remarkable features of the low-thrust solution are proven in Figs. 6d, 7d, and 8d: in this solution, the switching function S exhibits about 150 zero crossings, which cause 150 switching bang–bang structures in the throttle factor u and about the same number of revolutions. The values of $\boldsymbol{\lambda}_i$ that allows solving of problem (16) are reported in Table 5 for all of the four cases presented.

VI. Conclusions

In this work, the formulation of low-thrust minimum-fuel, minimum-energy, and minimum-time trajectories in the restricted three-body problem is discussed, with applications to transfers from a geostationary transfer orbit to a halo orbit about L_1 in the Earth–moon model. As these problems pose several challenges, a number of issues allowing an effective and efficient implementation of a solution method are discussed. These techniques involve solving the minimum-time problem, introducing energy-to-fuel homotopy, formulating analytical derivatives, and implementing a hybrid method for accurate switching point detection.

A fixed point of the halo is targeted without exploiting its stable manifold. The algorithm is left free to place thrust arcs everywhere, and the existence of free coast arcs, mimicking the stable manifold, is found a posteriori. To the best of the authors' knowledge, these techniques have enabled solving, for the first time, the geostationary transfer orbit to halo low-thrust transfer entirely, so avoiding splitting up the transfers into phases, which involves suboptimality.

Acknowledgments

C. Zhang would like to acknowledge the support provided by the China Scholarship Council. This work was supported by the National Natural Science Foundation of China (grant no. 11102007).

References

[1] Mingotti, G., Topputo, F., and Bernelli-Zazzera, F., "Optimal Low-Thrust Invariant Manifold Trajectories via Attainable Sets," *Journal of Guidance, Control, and Dynamics*, Vol. 34, No. 6, 2011, pp. 1644–1656. doi:10.2514/1.52493

[2] Mingotti, G., and Gurfil, P., "Mixed Low-Thrust Invariant-Manifold Transfers to Distant Prograde Orbits Around Mars," *Journal of Guidance, Control, and Dynamics*, Vol. 33, No. 6, 2010, pp. 1753–1764. doi:10.2514/1.49810

[3] Anderson, R., and Lo, M., "Role of Invariant Manifolds in Low-Thrust Trajectory Design," *Journal of Guidance, Control, and Dynamics*, Vol. 32, No. 6, 2009, pp. 1921–1930. doi:10.2514/1.37516

[4] Mingotti, G., Topputo, F., and Bernelli-Zazzera, F., "Low-Energy, Low-Thrust Transfers to the Moon," *Celestial Mechanics and Dynamical Astronomy*, Vol. 105, Nos. 1–3, 2009, pp. 61–74. doi:10.1007/s10569-009-9220-7

[5] Mingotti, G., Topputo, F., and Bernelli-Zazzera, F., "Efficient Invariant-Manifold, Low-Thrust Planar Trajectories to the Moon," *Communications in Nonlinear Science and Numerical Simulation*, Vol. 17, No. 2, 2012, pp. 817–831. doi:10.1016/j.cnsns.2011.06.033

[6] Pierson, B., and Kluever, C., "Three-Stage Approach to Optimal Low-Thrust Earth–Moon Trajectories," *Journal of Guidance, Control, and Dynamics*, Vol. 17, No. 6, 1994, pp. 1275–1282. doi:10.2514/3.21344

[7] Kluever, C., and Pierson, B., "Optimal Low-Thrust Three-Dimensional Earth–Moon Trajectories," *Journal of Guidance, Control, and*

Table 5 Initial costate λ_i and final time t_f for the four minimum-fuel solutions presented

T_{max}	$\boldsymbol{\lambda}_{r,i}$	$\boldsymbol{\lambda}_{v,i}$	$\lambda_{m,i}$	t_f, days
10 N	$[15.616017, 32.875896, -0.094522]^\top$	$[-0.101606, 0.044791, -0.000150]^\top$	0.133266	8.6
2 N	$[6.476119, 13.589566, 0.133954]^\top$	$[-0.041598, 0.018240, -0.000162]^\top$	0.126720	37.8
1 N	$[4.229762, 10.873196, -0.420268]^\top$	$[-0.030411, 0.016232, 0.000094]^\top$	0.123321	84.3
0.6 N	$[3.728251, 9.861519, -0.412042]^\top$	$[-0.027239, 0.014900, -0.000007]^\top$	0.122115	140.2

Dynamics, Vol. 18, No. 4, 1995, pp. 830–837.
doi:10.2514/3.21466

[8] Herman, A., and Conway, B., "Optimal, Low-Thrust, Earth–Moon Orbit Transfer," *Journal of Guidance, Control, and Dynamics*, Vol. 21, No. 1, 1998, pp. 141–147.
doi:10.2514/2.4210

[9] Russell, R., "Primer Vector Theory Applied to Global Low-Thrust Trade Studies," *Journal of Guidance, Control, and Dynamics*, Vol. 30, No. 2, 2007, pp. 460–472.
doi:10.2514/1.22984

[10] Caillau, J., Daoud, B., and Gergaud, J., "Minimum Fuel Control of the Planar Circular Restricted Three-Body Problem," *Celestial Mechanics and Dynamical Astronomy*, Vol. 114, Nos. 1–2, 2012, pp. 137–150.
doi:10.1007/s10569-012-9443-x

[11] Schoenmaekers, J., Horas, D., and Pulido, J., "SMART-1: With Solar Electric Propulsion to the Moon," *Proceeding of the 16th International Symposium on Space Flight Dynamics*, NASA Jet Propulsion Lab., Pasadena, CA, 2001, pp. 1–14.

[12] Belbruno, E., "Lunar Capture Orbits, a Method of Constructing Earth–Moon Trajectories and the Lunar GAS Mission," *Proceedings of the AIAA/DGLR/JSASS International Electric Propulsion Conference*, AIAA Paper 1987-1054, 1987, pp. 97–1054.

[13] Condon, G., and Pearson, D., "The Role of Humans in Libration Point Missions with Specific Application to an Earth–Moon Libration Point Gateway Station," *Advances in the Astronautical Sciences*, Vol. 109, AAS Paper 2001-307, Univelt, San Diego, CA, 2001, pp. 95–110.

[14] Farquhar, R., Dunham, D., Guo, Y., and McAdams, J., "Utilization of Libration Points for Human Exploration in the Sun–Earth–Moon System and Beyond," *Acta Astronautica*, Vol. 55, Nos. 3–9, 2004, pp. 687–700.
doi:10.1016/j.actaastro.2004.05.021

[15] Post, K., Belbruno, E., and Topputo, F., "Efficient Cis-Lunar Trajectories," *Global Space Exploration Conference*, International Astronautical Federation Paper GLEX-2012.02.3.6x12248, Paris, 2012, pp. 1–19.

[16] Mingotti, G., Topputo, F., and Bernelli-Zazzera, F., "Combined Optimal Low-Thrust and Stable-Manifold Trajectories to the Earth–Moon Halo Orbits," *AIP Conference Proceedings*, Vol. 886, AIP Publ., College Park, MD, 2007, pp. 100–110.
doi:10.1063/1.2710047

[17] Armellin, R., and Topputo, F., "A Sixth-Order Accurate Scheme for Solving Two-Point Boundary Value Problems in Astrodynamics," *Celestial Mechanics and Dynamical Astronomy*, Vol. 96, Nos. 3–4, 2006, pp. 289–309.
doi:10.1007/s10569-006-9047-4

[18] Martin, C., and Conway, B., "Optimal Low-Thrust Trajectories Using Stable Manifolds," *Spacecraft Trajectory Optimization*, Cambridge Univ. Press, Cambridge, England, U.K., 2010, pp. 238–262.

[19] Pergola, P., Finocchietti, C., and Andrenucci, M., "Design of Low-Thrust Transfers to Libration Point Periodic Orbits Exploiting Manifold Dynamics," *Advances in the Astronautical Sciences*, Vol. 145, AAS Paper 2012-330, Univelt, San Diego, CA, 2012, pp. 421–436.

[20] Rasotto, M., Armellin, R., Di Lizia, P., and Bernelli-Zazzera, F., "Optimal Low-Thrust Transfers in Two-Body and Three-Body Dynamics," *64th International Astronautical Congress*, Curran Assoc., Red Hook, NY, 2013, pp. 5230–5244.

[21] Starchville, T., and Melton, R., "Optimal Low-Thrust Trajectories to Earth–Moon L2 Halo Orbits (Circular Problem)," *Proceedings of the AAS/AIAA Astrodynamics Specialists Conference*, American Astronomical Soc., Sun Valley, ID, 1997, pp. 97–714.

[22] Senent, J., Ocampo, C., and Capella, A., "Low-Thrust Variable-Specific-Impulse Transfers and Guidance to Unstable Periodic Orbits," *Journal of Guidance, Control, and Dynamics*, Vol. 28, No. 2, 2005, pp. 280–290.
doi:10.2514/1.6398

[23] Ozimek, M., and Howell, K., "Low-Thrust Transfers in the Earth–Moon System Including Applications to Libration Point Orbits," *Journal of Guidance, Control, and Dynamics*, Vol. 33, No. 2, 2010, pp. 533–549.
doi:10.2514/1.43179

[24] Abraham, A., Spencer, D., and Hart, T., "Preliminary Optimization of Low-Thrust, Geocentric to Halo Orbit, Transfers via Particle Swarm Optimization," *24th AAS/AIAA Space Flight Mechanics Meeting*, Univelt, San Diego, CA, Jan. 2014, pp. 1–17.

[25] Caillau, J., and Daoud, B., "Minimum Time Control of the Restricted Three-Body Problem," *SIAM Journal on Control and Optimization*, Vol. 50, No. 6, 2012, pp. 3178–3202.
doi:10.1137/110847299

[26] Bertrand, R., and Epenoy, R., "New Smoothing Techniques for Solving Bang–Bang Optimal Control Problems: Numerical Results and Statistical Interpretation," *Optimal Control Applications and Methods*, Vol. 23, No. 4, 2002, pp. 171–197.
doi:10.1002/oca.709

[27] Haberkorn, T., Martinon, P., and Gergaud, J., "Low Thrust Minimum-Fuel Orbital Transfer: a Homotopic Approach," *Journal of Guidance, Control, and Dynamics*, Vol. 27, No. 6, 2004, pp. 1046–1060.
doi:10.2514/1.4022

[28] Jiang, F., Baoyin, H., and Li, J., "Practical Techniques for Low-Thrust Trajectory Optimization with Homotopic Approach," *Journal of Guidance, Control, and Dynamics*, Vol. 35, No. 1, 2012, pp. 245–258.
doi:10.2514/1.52476

[29] Martinon, P., and Gergaud, J., "SHOOT2.0: An Indirect Grid Shooting Package for Optimal Control Problems, with Switching Handling and Embedded Continuation," Inst. National de Recherche en Informatique et an Automatique, TR-7380, Inria Saclay, France, 2010.

[30] Mantia, L., and Casalino, L., "Indirect Optimization of Low-Thrust Capture Trajectories," *Journal of Guidance, Control, and Dynamics*, Vol. 29, No. 4, 2006, pp. 1011–1014.
doi:10.2514/1.18986

[31] Casalino, L., Colasurdo, G., and Pastrone, D., "Optimal Low-Thrust Escape Trajectories Using Gravity Assist," *Journal of Guidance, Control, and Dynamics*, Vol. 22, No. 5, 1999, pp. 637–642.
doi:10.2514/2.4451

[32] Szebehely, V., *Theory of Orbits: The Restricted Problem of Three Bodies*, Academic Press, New York, 1967, pp. 7–29.

[33] Prussing, J., "Primer Vector Theory and Applications," *Spacecraft Trajectory Optimization*, Cambridge Univ. Press, Cambridge, England, U.K., 2010, pp. 16–36.

[34] Thevenet, B., and Epenoy, R., "Minimum-Fuel Deployment for Spacecraft Formations via Optimal Control," *Journal of Guidance, Control, and Dynamics*, Vol. 31, No. 1, 2008, pp. 101–113.
doi:10.2514/1.30364

[35] Bryson, A., and Ho, Y., *Applied Optimal Control*, Wiley, New York, 1975, pp. 42–89.

[36] Pontryagin, L., *Mathematical Theory of Optimal Processes*, Interscience, New York, 1962, pp. 1–114.

[37] Lawden, D., *Optimal Trajectories for Space Navigation*, Butterworths, London, 1963, pp. 1–59.

This article has been cited by:

1. Zhemin Chi, Fanghua Jiang, Gao Tang. 2020. Optimization of variable-specific-impulse gravity-assist trajectories via optimality-preserving transformation. *Aerospace Science and Technology* **101**, 105828. [Crossref]
2. Roberto Furfaro, Daniele Mortari. 2020. Least-squares solution of a class of optimal space guidance problems via Theory of Connections. *Acta Astronautica* **168**, 92-103. [Crossref]
3. Roberto Furfaro, Andrea Scorsoglio, Richard Linares, Mauro Massari. 2020. Adaptive Generalized ZEM-ZEV Feedback Guidance for Planetary Landing via a Deep Reinforcement Learning Approach. *Acta Astronautica* . [Crossref]
4. Kshitij Mall, Ehsan Taheri. Unified Trigonometrization Method for Solving Optimal Control Problems in Atmospheric Flight Mechanics . [Abstract] [PDF] [PDF Plus]
5. Yuki Kayama, Mai Bando, Shinji Hokamoto. Minimum Fuel Trajectory Design Using Sparse Optimal Control in Three-Body Problem . [Abstract] [PDF] [PDF Plus]
6. Haiyang Li, Shiyu Chen, Dario Izzo, Hexi Baoyin. 2020. Deep networks as approximators of optimal low-thrust and multi-impulse cost in multitarget missions. *Acta Astronautica* **166**, 469-481. [Crossref]
7. Xun Pan, Binfeng Pan. 2020. Practical Homotopy Methods for Finding the Best Minimum-Fuel Transfer in the Circular Restricted Three-Body Problem. *IEEE Access* **8**, 47845-47862. [Crossref]
8. Mohammadreza Saghamanesh, Ehsan Taheri, Hexi Baoyin. 2019. Systematic low-thrust trajectory design to Mars based on a full Ephemeris modeling. *Advances in Space Research* **64**:11, 2356-2378. [Crossref]
9. Yongfei Gao, Zhaokui Wang, Yulin Zhang. 2019. Low thrust Earth–Moon transfer trajectories via lunar capture set. *Astrophysics and Space Science* **364**:12. . [Crossref]
10. Taibo Li, Zhaokui Wang, Yulin Zhang. 2019. Double-homotopy technique for fuel optimization of power-limited interplanetary trajectories. *Astrophysics and Space Science* **364**:9. . [Crossref]
11. Juan L. Gonzalo, Claudio Bombardelli. 2019. Optimal Constant-Thrust Radius Change in Circular Orbit. *Journal of Guidance, Control, and Dynamics* **42**:8, 1693-1708. [Abstract] [Full Text] [PDF] [PDF Plus]
12. Binfeng Pan, Yangyang Ma, Yang Ni. 2019. A new fractional homotopy method for solving nonlinear optimal control problems. *Acta Astronautica* **161**, 12-23. [Crossref]
13. Lingchao Zhu, Jian Ma, Shuquan Wang. 2019. Deep Neural Networks Based Real-time Optimal Control for Lunar Landing. *IOP Conference Series: Materials Science and Engineering* **608**, 012045. [Crossref]
14. Liqiang Hou, Shufan Wu, Zhaohui Hou, Zhongcheng Mu. Low-Thrust Trajectory Design Optimization with Stochastic Convolution 3380-3387. [Crossref]
15. Badaoui El Mabsout, Pierre Claudé, Michel Dudeck. 2019. Rendezvous of a continuous low-thrust cubesat with a satellite. *Journal of Physics Communications* **3**:5, 055014. [Crossref]
16. Chang Liu, Lu Dong. 2019. Physics-based control education: energy, dissipation, and structure assignments. *European Journal of Physics* **40**:3, 035006. [Crossref]
17. Binfeng Pan, Xun Pan, Yangyang Ma. 2019. A quadratic homotopy method for fuel-optimal low-thrust trajectory design. *Proceedings of the Institution of Mechanical Engineers, Part G: Journal of Aerospace Engineering* **233**:5, 1741-1757. [Crossref]
18. Yazhe Meng, Hao Zhang, Yang Gao. 2019. Low-Thrust Minimum-Fuel Trajectory Optimization Using Multiple Shooting Augmented by Analytical Derivatives. *Journal of Guidance, Control, and Dynamics* **42**:3, 662-677. [Citation] [Full Text] [PDF] [PDF Plus]
19. Bindu B. Jagannatha, Jean-Baptiste H. Bouvier, Koki Ho. 2019. Preliminary Design of Low-Energy, Low-Thrust Transfers to Halo Orbits Using Feedback Control. *Journal of Guidance, Control, and Dynamics* **42**:2, 260-271. [Abstract] [Full Text] [PDF] [PDF Plus]
20. John L. Junkins, Ehsan Taheri. 2019. Exploration of Alternative State Vector Choices for Low-Thrust Trajectory Optimization. *Journal of Guidance, Control, and Dynamics* **42**:1, 47-64. [Abstract] [Full Text] [PDF] [PDF Plus]
21. Ashish Tewari. Flight in Non-spherical Gravity Fields 199-252. [Crossref]
22. Francesco Topputo, Simone Ceccherini. A Catalogue of Parametric Time-Optimal Transfers for All-Electric GEO Satellites 459-478. [Crossref]
23. Pooja Dutt. 2018. A review of low-energy transfers. *Astrophysics and Space Science* **363**:12. . [Crossref]

24. Mohammadreza Saghamanesh, Hexi Baoyin. 2018. A robust homotopic approach for continuous variable low-thrust trajectory optimization. *Advances in Space Research* **62**:11, 3095-3113. [Crossref]
25. Binfeng Pan, Xun Pan, Siqi Zhang. 2018. A new probability-one homotopy method for solving minimum-time low-thrust orbital transfer problems. *Astrophysics and Space Science* **363**:9. . [Crossref]
26. Chuanmin Guo, Jin Zhang, Yazhong Luo, Luyi Yang. 2018. Phase-matching homotopic method for indirect optimization of long-duration low-thrust trajectories. *Advances in Space Research* **62**:3, 568-579. [Crossref]
27. Kui Zeng, Baolin Wu, Yunhai Geng. 2018. Two-phase shaping approach to low-thrust trajectories design between coplanar orbits. *Advances in Space Research* **62**:3, 593-613. [Crossref]
28. Zhemin Chi, Haiyang Li, Fanghua Jiang, Junfeng Li. 2018. Power-limited low-thrust trajectory optimization with operation point detection. *Astrophysics and Space Science* **363**:6. . [Crossref]
29. Paolo Massioni, Mauro Massari. 2018. Convex optimisation approach to constrained fuel optimal control of spacecraft in close relative motion. *Advances in Space Research* **61**:9, 2366-2376. [Crossref]
30. Maxime Chupin, Thomas Haberkorn, Emmanuel Trélat. 2018. Transfer Between Invariant Manifolds: From Impulse Transfer to Low-Thrust Transfer. *Journal of Guidance, Control, and Dynamics* **41**:3, 658-672. [Abstract] [Full Text] [PDF] [PDF Plus]
31. Daniel Pérez-Palau, Richard Epenoy. 2018. Fuel optimization for low-thrust Earth–Moon transfer via indirect optimal control. *Celestial Mechanics and Dynamical Astronomy* **130**:2. . [Crossref]
32. Lin Cheng, Zhenbo Wang, Fanghua Jiang, Chengyang Zhou. 2018. Real-Time Optimal Control for Spacecraft Orbit Transfer via Multi-Scale Deep Neural Networks. *IEEE Transactions on Aerospace and Electronic Systems* 1. [Crossref]
33. Mingcheng Zuo, Guangming Dai, Lei Peng. 2017. EP_DE II: A significant algorithm to search the optimal solution for global optimization of multi-gravity assist trajectory. *Proceedings of the Institution of Mechanical Engineers, Part G: Journal of Aerospace Engineering* **51**, 095441001771400. [Crossref]
34. Helen C. Henninger, James D. Biggs. 2017. Near Time-Minimal Earth to L1 Transfers for Low-Thrust Spacecraft. *Journal of Guidance, Control, and Dynamics* **40**:11, 2999-3004. [Citation] [Full Text] [PDF] [PDF Plus]
35. Zhemin Chi, Hongwei Yang, Shiyu Chen, Junfeng Li. 2017. Homotopy method for optimization of variable-specific-impulse low-thrust trajectories. *Astrophysics and Space Science* **362**:11. . [Crossref]
36. Shuge Zhao, Jingrui Zhang, Kaiheng Xiang, Rui Qi. 2017. Target sequence optimization for multiple debris rendezvous using low thrust based on characteristics of SSO. *Astrodynamics* **1**:1, 85-99. [Crossref]
37. Zhengfan Zhu, Qingbo Gan, Xin Yang, Yang Gao. 2017. Solving fuel-optimal low-thrust orbital transfers with bang-bang control using a novel continuation technique. *Acta Astronautica* **137**, 98-113. [Crossref]
38. Kenta Oshima, Stefano Campagnola, Tomohiro Yanao. 2017. Global search for low-thrust transfers to the Moon in the planar circular restricted three-body problem. *Celestial Mechanics and Dynamical Astronomy* **128**:2-3, 303-322. [Crossref]
39. Maxime Chupin, Thomas Haberkorn, Emmanuel Trélat. 2017. Low-thrust Lyapunov to Lyapunov and Halo to Halo missions with L 2 -minimization. *ESAIM: Mathematical Modelling and Numerical Analysis* **51**:3, 965-996. [Crossref]
40. Bruno Victorino Sarli, Yasuhiro Kawakatsu. 2017. Selection and trajectory design to mission secondary targets. *Celestial Mechanics and Dynamical Astronomy* **127**:2, 233-258. [Crossref]
41. Hanlun Lei, Bo Xu, Lei Zhang. 2017. Trajectory design for a rendezvous mission to Earth's Trojan asteroid 2010 TK 7. *Advances in Space Research* **60**:11, 2505. [Crossref]
42. ShuGe Zhao, Pini Gurfil, JingRui Zhang. 2016. Initial Costates for Low-Thrust Minimum-Time Station Change of Geostationary Satellites. *Journal of Guidance, Control, and Dynamics* **39**:12, 2746-2756. [Citation] [Full Text] [PDF] [PDF Plus]
43. Zheng Chen. 2016. $$\mathrm{L}^1$$ L 1 -optimality conditions for the circular restricted three-body problem. *Celestial Mechanics and Dynamical Astronomy* **126**:4, 461-481. [Crossref]
44. ShuGe Zhao, JingRui Zhang. 2016. Minimum-fuel station-change for geostationary satellites using low-thrust considering perturbations. *Acta Astronautica* **127**, 296-307. [Crossref]
45. Zhaohui Dang, Shengyong Tang, Min Hu. Some integrals observed in spacecraft relative motion problem with circular reference orbit 2450-2455. [Crossref]
46. Jean-Baptiste Caillau, Ariadna Farrés. On Local Optima in Minimum Time Control of the Restricted Three-Body Problem 209-302. [Crossref]

47. Gao Tang, Fanghua Jiang. 2016. Capture of near-Earth objects with low-thrust propulsion and invariant manifolds. *Astrophysics and Space Science* **361**:1. . [Crossref]